Fushimi, T., Hill, T. L., Marzo, A., & Drinkwater, B. W. (2018). Nonlinear trapping stiffness of mid-air single-axis acoustic levitators. *Applied Physics Letters*, *113*(3), [034102]. https://doi.org/10.1063/1.5034116

Nonlinear Trapping Stiffness of Mid-Air Single-Axis Acoustic Levitators

T. Fushimi,[a] T. L. Hill, A. Marzo, and B. W. Drinkwater

Department of Mechanical Engineering, University of Bristol, BS8 1TR, Bristol, United Kingdom

(Dated: 10 July 2018)

We describe and experimentally explore a nonlinear stiffness model of the trapping of a solid particle in a single-axis acoustic levitator. In contrast to the commonly employed linear stiffness assumption, our nonlinear model accurately predicts the response of the system. Our nonlinear model approximates the acoustic field in the vicinity of the trap as a one-dimensional sinusoid and solves the resulting dynamics using numerical continuation. In particular, we predict a softening of stiffness with amplitude as well as period-doubling bifurcations, even for small excitation amplitudes of $\approx 2\%$ of the wavelength. These nonlinear dynamic features are observed experimentally in a single-axis levitator operating at 40 kHz and trapping millimetre-scale expanded polystyrene spheres. Excellent agreement between the observed and predicted behaviour is obtained suggesting that this relatively simple model captures the relevant physical phenomena. This new model enables the dynamic instabilities of trapped particles to be accurately predicted thereby benefiting contactless transportation and manipulation applications.

[a] Electronic mail: t.fushimi@bristol.ac.uk

Acoustic radiation forces are hydrodynamic forces exerted through the interaction of the acoustic field with the particles contained in it[1–5]. Devices which can levitate or manipulate objects using acoustic radiation forces are typically referred to as acoustic levitators. Acoustic levitators can be categorized into four main classes[6]: single-axis standing wave, multi-axis, near-field and single-beam. The single-axis standing wave levitator is a classical method for contactlessly holding samples, it is commonly realized by a Langevin horn and another opposed horn or reflector[7] as shown in FIG. 1 (a). Recently, it has been shown that an array of transducers can also create pseudo-one-dimensional standing waves with the added advantage of controlling the position of the nodes along the propagation axis[8,9], as illustrated in FIG. 1 (b). However, in all these cases, a pseudo-one-dimensional standing wave is generated and the particles are trapped at the nodes with sinusoidal restoring forces as shown in FIG. 1 (c).

Acoustic levitators have a broad range of applications in non-contact transportation and as a processing method for pharmaceutical, biological or chemical applications[10–15]. The behaviour of the levitated objects has been of interest in all classes of acoustic levitator[16–18]. The chaotic shape dynamics of bubbles and droplets inside acoustic levitators are well documented[19,20] and the translational oscillation of these deformable samples has been studied in the past, often with damping forces neglected[21–23]. Perez et al.[24] devised an experimental approach to determine the dynamics of solid particles in a standing wave levitator and demonstrated the fit of quadratic damping terms in a dynamic model. Jia et al. analyzed the dynamic response of micro-particles in liquids to show the effects of acoustic streaming and hydrodynamic forces on particles[25] and Andrade et al.[26] pointed out that the particle may exhibit nonlinear behaviours similar to a Duffing oscillator. However, the dynamics of solid particles suspended inside a standing wave levitator in mid-air have not yet been fully explored, the majority of recent research employs linear stiffness models[24,27–30] which are applicable only in the case that the movement of the suspended particle is small[6]. The lack of understanding of the translational dynamics of the levitated samples hinders the development of future applications with acoustic levitators where the small displacement assumption is no longer valid. This prevents accurate prediction of the particle dynamics.

Here, we present a nonlinear dynamic model for the restoring forces inside a single-axis acoustic levitator. The model accurately predicts various nonlinear dynamic phenomena such as amplitude-dependence, multiple solutions, and period-doubling bifurcations. These

responses were then observed experimentally, and found to be in excellent agreement with our predictions whereas previous linear stiffness models by definition, fail to predict these phenomena.

The experiment discussed here consists of a solid sphere suspended against gravity at the central node of a multi-transducer standing wave acoustic levitator operating at 40 kHz, as shown in FIG. 2 (see supplementary material for further details on the pressure field calculation). This device is an instance of the general class of single axis standing wave levitator depicted in FIG. 1 (b). The acoustic radiation force was numerically approximated using the Gor'kov potential assuming that the particle (EPS, $\rho_p = 34.0\,\mathrm{kg\,m^{-3}}$) is small (radius, $r = 0.71 \pm 0.03\,\mathrm{mm}$) in comparison to the wavelength[5,31] ($\lambda = 8.6\,\mathrm{mm}$). The particle used in the experiment was visually inspected for deformations, the roundness of the particle was measured as 0.938 (see supplementary material).

The restoring force in the vicinity of the equilibrium point for the central node in the acoustic levitator is approximated as a sinusoidal force function, assuming that acoustic radiation force only varies with the vertical displacement (z):

$$F_{rad} = \alpha \sin\left(\beta(z - z_p)\right) \tag{1}$$

where $\alpha = -3.06 \times 10^{-6}\,\mathrm{N}$, $\beta = 1315\,\mathrm{m^{-1}}$ are the constants, obtained from a fit to the simulated pressure field (pressure amplitude $\approx 800\,\mathrm{Pa}$ at 5 V) in the vicinity of the central node (see supplementary material). z is the particle position measured from an arbitrary origin on the z-axis, z_p is the input perturbation. The input perturbation represents an

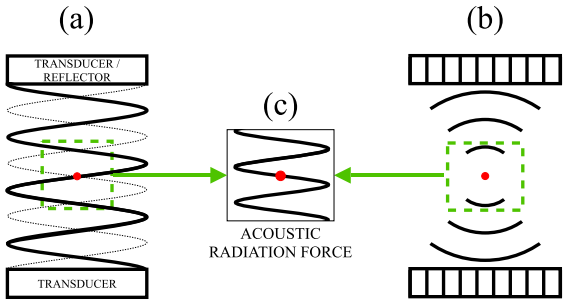

FIG. 1. Two types of single-axis standing wave levitators. (a) A Langevin transducer assembly with an opposed reflector, or another transducer. (b) Two transducer arrays with phase delays or geometry designed to focus the acoustic waves at the center. (c) Resultant central pseudo-one-dimensional sinusoidal acoustic radiation force from both of the acoustic levitators.

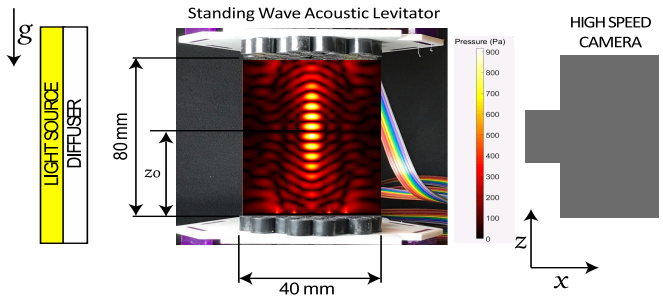

FIG. 2. Schematic of the experimental setup. On the left, there is a light with a diffuser for illumination. In the center, the multi-element standing wave levitator traps a particle in the center, it also changes the phase-delays to move the central trap in the z direction. The numerically calculated pressure amplitude field (see supplementary material) is shown overlaid. On the right, a high-speed camera captures the particle motion.

excitation either by a mechanical vibration, e.g. from a shaker, or by changing the acoustic pressure field to move the nodal position. In the experiment, the latter method was used and the acoustic pressure field was varied by changing the focal point of the phased-array, thus moving the nodal positions of the standing wave. For a small value of z_p, equation (1) is analogous to a base-excited pendulum[32–35] and the input perturbation can be considered as a parametric excitation (see supplementary material). In comparison, the commonly employed linear model of this system is identified by finding the linear stiffness (K_L) around the equilibrium point, which can be calculated by differentiating F_{rad} over z which gives[6]:

$$F_{rad,L} = -K_L(z - z_p) \tag{2}$$

where $K_L = 0.0397\,\mathrm{Nm}^{-1}$.

The dynamics of the system can be explored by approaches such as the random excitation, sine-sweep, or a stepped sine-sweep[36]. Here, a stepped-sine method was used and by varying the focal point with a sinusoidal function ($z_p = z_o + A_{in}\sin(2\pi\Omega t)$) at a constant frequency (Ω), z-axis offset (z_0) and amplitude (A_{in}). The coefficients given in equation (1) hold true with minimum R^2=0.998 for the range of $z - z_p$ shown in this paper. The damping force was calculated as[37,38]: $F_{drag} = -\frac{1}{2}C_d\frac{\pi}{4}(2r)^2\rho_a\,|\dot{z}|\,\dot{z}$, where the damping coefficient is $C_d = \frac{24}{\mathrm{Re}}\sqrt{1+\frac{3}{16}\mathrm{Re}}$, and where $\mathrm{Re} = (2r|\dot{z}|\,\rho_a)/\mu$ is the Reynolds number. This is applicable for $\mathrm{Re} \leq 100$ and assumes that history forces and added mass are negligible in air.

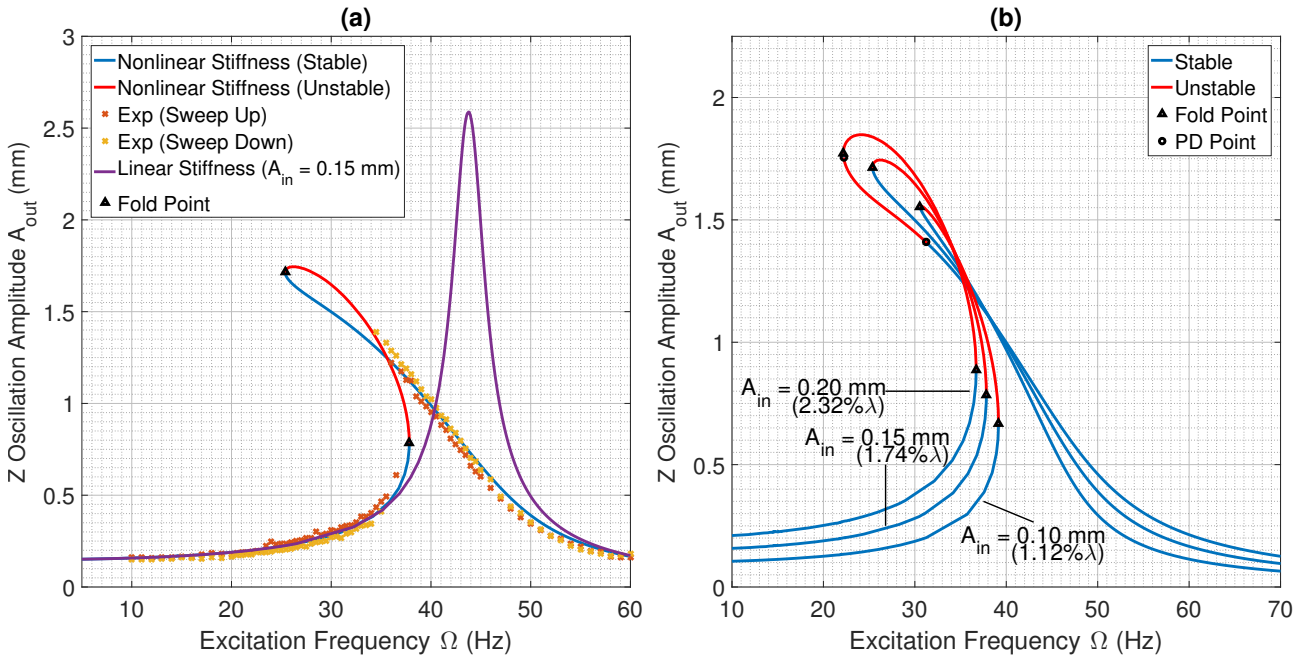

FIG. 3. Predicted and experimental response of a particle trapped in a standing wave levitator. (a) Comparison of the nonlinear stiffness model, experimental results and equivalent linear stiffness model with $A_{in} = 0.15\,\text{mm}$. (b) Predicted response from the nonlinear model when excited at different amplitudes.

Balancing the inertial and force components gives:

$$m\ddot{z} = (F_{rad} + F_{grav}) + F_{drag} \tag{3}$$

where $F_{grav} = -mg$ is the gravitational force and F_{rad} is given by equation (1). For a linear stiffness model, the forces inside the bracket are replaced by equation (2). Equation (3) was solved using the numerical continuation software Continuation Core and Toolboxes (COCO)[39] in MATLAB, to predict the dynamic response for both linear and nonlinear stiffness models. Numerical continuation is widely employed in the field of nonlinear dynamics[40] and it can be used to compute periodic solutions, determine their stability and identify bifurcations[39]. These solutions may be considered accurate to within the tolerances of the numerical solver. One drawback in the use of numerical tools, in comparison to analytical approaches, is that they reveal less about the nature and root cause of the dynamic behaviour. However, such a study is beyond the scope of the current work.

In order to conduct an experimental verification of the proposed dynamic model, the acoustic levitator was set up as shown in FIG. 2. The vertical dynamic manipulation of the

focal point is transmitted from the computer to the acoustic levitator driver board at 700 Hz via a UART serial communication line operating at 500 kbauds. The driver board is made of an FPGA board (ALTERA CoreEp4CE6) which generates 60 independent square waves with a phase resolution of $\phi = \frac{2\pi}{128}$. These signals were amplified up to 17 V by individual MOSFET drivers (TC4427a) powered with an external DC supply (RS Pro IPS 303DD). The amplified signals were fed into the levitator transducers (Murata MA40S4S). Despite the square excitation signals the output waves were sinusoidal due to the narrowband nature of the transducers[41].

The experiment was conducted in a chamber (width = 4.3 m, height = 2.4 m, length = 2.4 m) on a passive vibration isolation table (Thorlabs PFH90150-8) to minimize external air and vibration disturbances. Furthermore, the temperature, barometric pressure, and humidity were recorded at the beginning of each experiment and the numerical model was calibrated accordingly to accommodate the changes. At 21.3°C, the values of air density (ρ_a), viscosity (μ) and speed of sound (c_0) were $1.19\,\mathrm{kg\,m^{-3}}$, $1.82\times10^{-5}\,\mathrm{kg\,(m\,s)^{-1}}$, and $344\,\mathrm{m\,s^{-1}}$, respectively. The movement of the particle was captured by a high speed camera (Photoron FASTCAM SA-Z Type 2100K-M-32GB) and the silhouette of the levitated particle was recorded at a sampling frequency of 1001 Hz. The camera was calibrated using a CMM-stylus (Renishaw A-5000-7806) to find the pixel-to-meter conversion ($3.29\times10^{-5}\,\mathrm{m\,pix^{-1}}$). The high-speed camera data was processed by the MATLAB image analysis package to determine the center of the levitated particle, and the oscillation amplitude was obtained by taking the peak-to-peak difference of the low-pass filtered signal ($f_{pass} = 100\,\mathrm{Hz}$ and $f_{stop} = 150\,\mathrm{Hz}$).

The comparison of both numerical models (linear and nonlinear stiffness) and experimental results for $A_{in} = 0.15\,\mathrm{mm}$ are shown in FIG. 3 (a). The linear stiffness model predicts a symmetrical response around the resonance with a peak response amplitude of $A_{out} = 2.58\,\mathrm{mm}$. There are significant differences between this linear model and the experimental results even for a relatively small excitation amplitude of $A_{in} = 0.15\,\mathrm{mm}$ (or $1.74\%\lambda$). This is also small in comparison to the width of the Gor'kov potential, which is $4.8\,\mathrm{mm}$ ($A_{in} = 0.15\,\mathrm{mm}$ is 3.13% of the width of the local Gor'kov potential minima). On the other hand, the nonlinear stiffness model predicts the response of the system with a significantly greater accuracy of $R^2 = 0.998$ between model and experiment. Despite the small oscillation amplitude, the peak frequency predicted by the linear and nonlinear stiffness

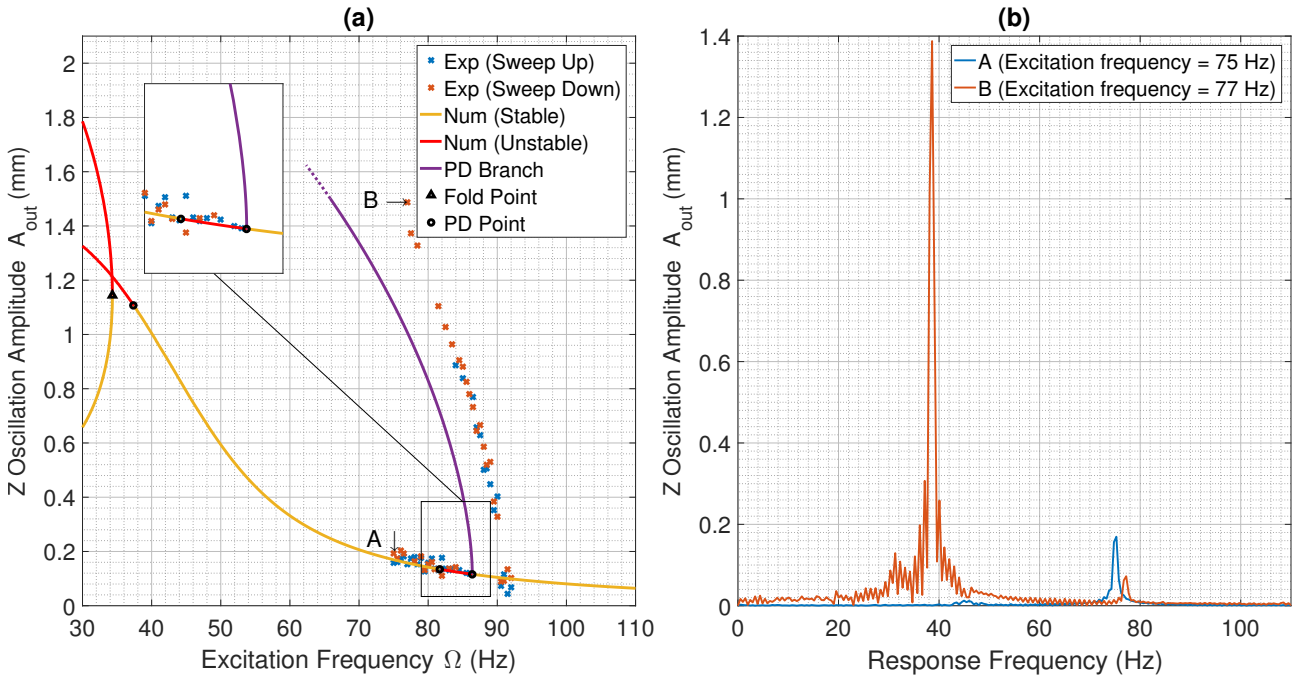

FIG. 4. Numerical model predicting period-doubling bifurcation. (a) The numerical model predicts an unstable response from 82 to 86 Hz, the experimental results confirm the existence of this period-doubling (PD) bifurcation. The PD branch is part of a stable region, and the dotted part continues to an unstable PD branch. (b) Frequency domain response of the signal denoted A and B in (a) from 'Exp (Sweep Down)'. The dominant frequency at point B, where the period-doubling is occurring, is half that of the excitation frequency, whereas point A oscillates at the excitation frequency. (Multimedia View)

models differ by ≈ 18 Hz. Moreover, the nonlinear stiffness model predicts fold bifurcations at the positions where stability changes, and experimental results in FIG. 3 (a) demonstrate that multiple stable solutions exist for certain forcing frequencies - a feature that is not seen in linear systems. Experimentally measuring the complete stable portion of the branch on the downwards sweep (between 25 Hz and 34 Hz) is challenging, as the basin of attraction of the stable response typically decreases as it approaches a fold bifurcation[42]. The red curve in FIG. 3 (a) represents unstable solutions, which cannot be measured experimentally, without employing a specific control strategy[43].

The nonlinear stiffness model exhibits amplitude-dependent behavior. The responses for excitation amplitudes $A_{in} = 0.10$, 0.15, and 0.20 mm were solved and are shown in FIG. 3 (b). Since the resonance frequency decreases with amplitude, the system is considered to be a

'softening' system[44]. The response becomes more symmetrical and approaches the linear stiffness model as the excitation amplitude decreases. This is caused by the reduction in the response amplitude of particle oscillation, which begins to meet the condition for a linear assumption. The linear stiffness model contains nonlinear damping terms, due to the drag forces, and therefore also exhibits amplitude dependence; however, the resonant frequency is independent of the excitation amplitude and hence still exhibits a characteristic symmetrical frequency response.

For large excitation amplitudes, a period-doubling (PD) bifurcation occurs near an excitation frequency of 80 Hz. For example, when the excitation amplitude is increased to $A_{in} = 0.35$ mm, an unstable region emerges between 82 and 86 Hz as shown in FIG. 4 (a); note that this bifurcation may also be observable at lower excitation amplitudes. A period-doubling bifurcation marks the point at which the response of the system switches to a new behaviour with a period that is twice that of the original response[45]. In the case of the response shown in FIG. 4 (a) this leads to a loss of stability of the single-period solutions (represented by the red line), and an emergence of a new set of double-period solutions (purple line). The above experimental procedure was repeated for the same particle with an excitation amplitude of $A_{in} = 0.35$ mm. The response amplitude increases significantly from 77 Hz to 90 Hz, with $A_{out} = 1.49$ mm. Although the experimentally obtained results are offset from the predicted period-doubling branch by ≈ 4 Hz, they show the same qualitative behaviour, verifying the existence of the PD bifurcation and resulting behaviour. An example of the frequency-dependence of the oscillatory response of the particle is available in the supplementary material. The frequency domain response of the signal for the points denoted A and B from 'Exp (Sweep Down)' on FIG. 4 (a) were measured and are shown in FIG. 4 (b) (Multimedia View). As the result of the period-doubling behavior, the dominant response frequency is at half of the excitation frequency, confirming the occurrence of a period-doubling bifurcation. Furthermore, as seen in FIG. 4 (a), period-doubling bifurcations may also occur at lower excitation frequencies, for example, period-doubling bifurcations occur at 37 Hz in FIG. 4 (a) and around 31 Hz for $A_{in} = 0.20$ mm in FIG. 3 (b). Due to the high amplitude of the response, the experimental confirmation of the low frequency period-doubling bifurcation has not yet been achieved. However, this indicates that more complex dynamics are possible and further investigation of the nonlinear dynamics of acoustic levitators is needed.

In conclusion, we experimentally validated a single degree-of-freedom nonlinear model of a solid particle trapped inside a mid-air single-axis levitator. We predicted and verified the occurrence of nonlinear softening behaviour, as well as period-doubling bifurcations. These behaviours were only predicted by the nonlinear stiffness model, highlighting the importance of the nonlinear model. Period doubling bifurcation is often the beginning of chaotic behaviour in many dynamic systems, and further studies may reveal this dynamic complexity in single-axis levitators. Nonlinear responses are caused by the characteristic sinusoidal restoring force, which is a common feature in acoustic levitators available in the literature. This new model enables the dynamic instabilities of trapped particles to be accurately predicted thereby benefiting contactless transportation and manipulation applications.

See supplementary material for the details on the array layout, the method for calculating the pressure field and acoustic radiation force, proof of similarity with a base-excited pendulum, particle properties and the approximation of a linear stiffness. A video of the particle at a period-doubling bifurcation is also available.

T.F. was funded through the Japan Student Services Organization (JASSO) Student Exchange Support Program (Graduate Scholarship for Degree Seeking Students). This project has been funded by the UK Engineering and Physical Science Research Council (EP/N014197/1). The authors would like to acknowledge the Bristol Composites Institute (ACCIS) for providing the high-speed camera. We would like to thank Dr. Andrew J. Harrison for his interesting discussions. Sufficient information is available in the manuscript and supplementary material to recreate the numerical and experimental results. The data presented in this work are openly available at Zenodo, https://doi.org/10.5281/zenodo.1306584

REFERENCES

[1]J. W. S. Rayleigh, The London, Edinburgh, and Dublin Philosophical Magazine and Journal of Science **3**, 338 (1902).

[2]J. W. S. Rayleigh, Philosophical Magazine Series 6 **10**, 364 (1905).

[3]L. V. King, Proc. R. Soc. A **147**, 212 (1934).

[4]K. Yosioka and Y. Kawasima, Acta Acustica united with Acustica **5**, 167 (1955).

[5]L. P. Gor'kov, Soviet Physics Doklady **6**, 773 (1962).

[6]M. A. B. Andrade, N. Pérez, and J. C. Adamowski, Brazilian Journal of Physics (2017), 10.1007/s13538-017-0552-6.

[7]R. R. Whymark, Ultrasonics **13**, 251 (1975).

[8]Y. Ochiai, T. Hoshi, and J. Rekimoto, PLoS ONE **9**, e97590 (2014).

[9]A. Marzo, A. Barnes, and B. W. Drinkwater, Review of Scientific Instruments **88**, 085105 (2017).

[10]C. J. Benmore and J. K. R. Weber, Physical Review X **1**, 1 (2011).

[11]D. Foresti, M. Nabavi, M. Klingauf, A. Ferrari, and D. Poulikakos, Proceedings of the National Academy of Sciences **110**, 12549 (2013), arXiv:arXiv:1507.02142v2.

[12]F. Guo, Z. Mao, Y. Chen, Z. Xie, J. P. Lata, P. Li, L. Ren, J. Liu, J. Yang, M. Dao, S. Suresh, and T. J. Huang, Proceedings of the National Academy of Sciences **113**, 1522 (2016).

[13]S. Tsujino and T. Tomizaki, Scientific Reports **6**, 1 (2016).

[14]L. Tian, N. Martin, P. G. Bassindale, A. J. Patil, M. Li, A. Barnes, B. W. Drinkwater, and S. Mann, Nature Communications **7**, 13068 (2016).

[15]B. W. Drinkwater, Lab Chip **16**, 2360 (2016).

[16]J. Rudnick and M. Barmatz, The Journal of the Acoustical Society of America **87**, 81 (1990).

[17]D. Foresti, M. Nabavi, and D. Poulikakos, Journal of Fluid Mechanics **709**, 581 (2012).

[18]D. Ilssar and I. Bucher, Journal of Applied Physics **121** (2017), 10.1063/1.4978365.

[19]R. G. Holt and L. A. Crum, The Journal of the Acoustical Society of America **91**, 1924 (1992).

[20]R. Mettin and A. A. Doinikov, Applied Acoustics **70**, 1330 (2009).

[21]Z. C. Feng and Y. H. Su, Physics of Fluids **9**, 519 (1997).

[22]E. H. Trinh and C. J. Hsu, The Journal of the Acoustical Society of America **80**, 1757 (1986).

[23]W. J. Xie and B. Wei, Physical Review E **70**, 046611 (2004).

[24]N. Pérez, M. A. B. Andrade, R. Canetti, and J. C. Adamowski, Journal of Applied Physics **116** (2014), 10.1063/1.4901579.

[25]K. Jia, D. Mei, J. Meng, and K. Yang, Journal of Applied Physics **116**, 164901 (2014).

[26]M. A. B. Andrade, T. S. Ramos, F. T. A. Okina, and J. C. Adamowski, Review of Scientific Instruments **85**, 045125 (2014).

[27]J. H. Xie and J. Vanneste, Physics of Fluids **26** (2014), 10.1063/1.4896523, arXiv:1406.3006.

[28]M. A. B. Andrade, N. Pérez, and J. C. Adamowski, The Journal of the Acoustical Society of America **136**, 1518 (2014).

[29]D. Foresti and D. Poulikakos, Physical Review Letters **112**, 024301 (2014), arXiv:arXiv:1507.02142v2.

[30]Z. Y. Hong, J. F. Yin, W. Zhai, N. Yan, W. L. Wang, J. Zhang, and B. W. Drinkwater, Sci. Rep. , 1 (2017).

[31]H. Bruus, Lab on a Chip **12**, 1014 (2012).

[32]Y. Liang and B. F. Feeny, Nonlinear Dynamics **46**, 17 (2006).

[33]J. M. Schmitt and P. V. Bayly, Nonlinear Dynamics **15**, 1 (1998).

[34]B. K. Donaldson, *Introduction to Structural Dynamics*, Cambridge Aerospace Series (Cambridge University Press, 2006).

[35]R. R. Soper, W. Lacarbonara, C.-M. Chin, A. H. Nayfeh, and D. T. Mook, Journal of Vibration and Control **7**, 1265 (2001), https://doi.org/10.1177/107754630100700808.

[36]R. Pintelon and J. Schoukens, *System Identification: A Frequency Domain Approach* (Wiley, 2012).

[37]J. Ward-Smith, *Mechanics of Fluids, Ninth Edition* (CRC Press, 2012).

[38]R. L. C. Flemmer and C. L. Banks, Powder Technology **48**, 217 (1986).

[39]H. Dankowicz and F. Schilder, *Recipes for Continuation*, Computational Science and Engineering (Society for Industrial and Applied Mathematics, 2013).

[40]B. Krauskopf, H. M. Osinga, and J. Galán-Vioque, *Numerical continuation methods for dynamical systems* (Springer, 2007).

[41]A. Marzo, T. Corkett, and B. W. Drinkwater, IEEE Transactions on Ultrasonics, Ferroelectrics, and Frequency Control **65**, 102 (2018).

[42]J. M. T. Thompson and H. B. Stewart, *Nonlinear Dynamics and Chaos* (Wiley, 2002).

[43]J. Sieber and B. Krauskopf, Nonlinear Dynamics **51**, 365 (2008).

[44]D. J. Wagg and S. A. Neild, *Nonlinear Vibration with Control: For Flexible and Adaptive Structures*, Solid Mechanics and Its Applications (Springer Netherlands, 2009).

[45]S. H. Strogatz, *Nonlinear Dynamics and Chaos: With Applications to Physics, Biology,*

Chemistry, and Engineering, Studies in nonlinearity (Westview Press, 2008) p. 360.